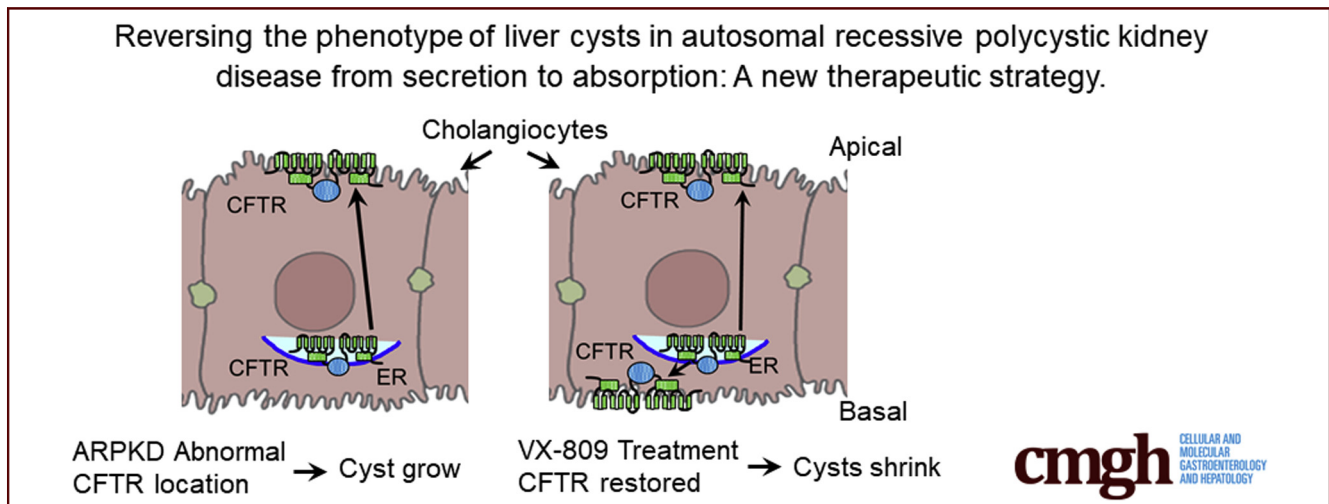## ORIGINAL RESEARCH

Therapeutic Potential for CFTR Correctors in Autosomal Recessive Polycystic Kidney Disease

Murali K. Yanda, Vartika Tomar, and Liudmila Cebotaru

Division of Gastroenterology and Hepatology, Department of Medicine, Johns Hopkins University School of Medicine, Baltimore, Maryland

Reversing the phenotype of liver cysts in autosomal recessive polycystic kidney disease from secretion to absorption: A new therapeutic strategy.

SUMMARY

Autosomal recessive polycystic kidney disease (ARPKD) causes severe disease in babies in the womb. Those who survive the neonatal period face chronic kidney and liver disease throughout their life. The overall goal of our study was to uncover therapeutic strategies to treat ARPKD.

BACKGROUND & AIMS: Autosomal recessive polycystic kidney disease (ARPKD) is caused by mutations in *PKHD1*, encoding fibrocystin/polyductin (FPC). Severe disease occurs in perinates. Those who survive the neonatal period face a myriad of comorbidities, including systemic and portal hypertension, liver fibrosis, and hepatosplenomegaly. The goal here was to uncover therapeutic strategies for ARPKD.

METHODS: We used wild-type and an FPC-mutant cholangiocyte cell line in 3-dimensional cysts and in confluent monolayers to evaluate protein expression using western blotting and protein trafficking using confocal microscopy.

RESULTS: We found that the protein level of the cystic fibrosis transmembrane conductance regulator (CFTR) was downregulated. The levels of heat shock proteins (HSPs) were altered in the FPC-mutant cholangiocytes, with HSP27 being downregulated and HSP90 and HSP70 upregulated. FPC-mutant cholangiocytes formed cysts, but normal cells did not. Cyst growth could be reduced by increasing HSP27 protein levels, by HSP90 and HSP70 inhibitor treatments, by silencing HSP90 through messenger RNA inhibition, or by the novel approach of treating the cysts with the CFTR corrector VX-809. In wild-type cholangiocytes, CFTR is present in both apical and basolateral membranes. FPC malfunction resulted in altered colocalization of CFTR with both apical and basolateral membranes. Whereas, treatment with VX-809, increasing HSP27 or inhibiting HSP70 or HSP90 restored CFTR localization toward normal values.

CONCLUSIONS: FPC malfunction induces the formation of cysts, which are fueled by alterations in HSPs and in CFTR protein levels and miss-localization. We suggest that CFTR correctors, already in clinical use to treat cystic fibrosis, could also be used as a treatment for ARPKD. *(Cell Mol Gastroenterol Hepatol 2021;12:1517–1529;* https://doi.org/10.1016/j.jcmgh.2021.07.012*)*

Autosomal recessive polycystic kidney disease (ARPKD) associated with mutations in PKHD1[1,2] is a debilitating autosomal recessive genetic disorder that is responsible for chronic end-stage renal disease in humans.[3,4] ARPKD[5] occurs in 1 in 20,000 live births in the United States. More than 350,000 people worldwide are affected each year, imposing a large health care burden and resulting in newborn morbidity and mortality. The most severe disease occurs in perinates, who present with massively enlarged, echogenic kidneys and oligohydramnios. Neonates with severe disease have pulmonary

hypoplasia and a mortality rate of ~30%.[6] Those who survive the neonatal period face a myriad of comorbidities, including systemic and portal hypertension, fibrosis of both the liver and kidney, hepatosplenomegaly,[3] and enlarged kidneys, with fusiform dilation of the collecting ducts that progresses to end-stage renal disease.[7] ARPKD is caused by mutations in the *PKHD1* gene, which encodes a large 4074-amino-acid protein, fibrocystin/polyductin (FPC), with a long extracellular domain and single transmembrane domain.[8,9] The existence of several alternate splicing forms suggest that FPC occurs as both an anchored and a secreted protein.[10] The gene is expressed predominantly in the fetal and adult liver, kidneys, and pancreas; the protein it encodes is present in the plasma membrane, primary cilium, and cytoplasm.[8] Consistent with its multilocational positioning, a functional deficit of FPC has been linked to a number of alterations in cellular integrity, such as changes in their cell adhesion, centrosome positioning, and ability to achieve correct polarization.[11]

Role of the Cystic Fibrosis Transmembrane Conductance Regulator in ARPKD

The cystic fibrosis transmembrane conductance regulator (CFTR) protein, whose mutation causes CF, has been suggested to also play a role in the growth of the cysts in autosomal dominant polycystic kidney disease (ADPKD). For example, O'Sullivan et al[12] reported that a patient cohort with both CF and ADPKD had less severe kidney and liver disease than did patients with ADPKD alone. On the other hand, Persu et al[13] were unable to find any difference in kidney volume or renal function between a cohort of ADPKD patients who also bore the F508-del CFTR mutation and a cohort of patients having ADPKD alone. Thus, the impact of CFTR on the progression of ADPKD is equivocal, with some studies pointing to some degree of amelioration and others showing no effect at all. However, in ARPKD, the role of CFTR appears to be quite different from its role in CF. For example, when Nakanishi et al[14] crossed a PBK mouse (an ARPKD model) with a CFTR-knockout mouse to create a bpk–/–;cftr–/– double homozygous mouse, they found, surprisingly, that the double mutants exhibited massively enlarged kidneys and died from renal failure at ~24 days after birth.[15] Therefore, we have now asked why knocking down CFTR apparently worsens the ARPKD disease phenotype.

Interestingly, liver disease is a frequent complication of CF that is present in about one-third of all CF patients[16] and has clear similarities to the liver disease observed in ARPKD. The clinical symptoms include biliary cirrhosis and progressive periportal fibrosis leading to portal hypertension and liver failure.[16] The classic thinking is that cholangitis in CF patients is caused by biliary obstruction that results from a deficit in fluid secretion via CFTR and other Cl- channels.[17] However, this notion has been questioned. For example, careful electron micrographic examination of liver pathology in patients with varying degrees of liver disease does not support the theory of chronic bile duct obstruction; instead, it shows evidence of increases in collagen deposition and cell proliferation and an abnormal cholangiocyte

morphology.[18] The authors of the study concluded that their findings do not support obstruction as a major factor in the development of fibrosis in CF.[19] Thus, one possible reason that mice with knockout of both CF and FPC exhibit worse disease is the added tendency to liver pathology in both diseases.

Role of Proteostasis

It is well known that an ensemble of proteins referred to as the proteostatic network plays a role in the normal processing of proteins.[20,21] According to Balch et al,[22] this network participates in disease processes. For example, the heat shock proteins (HSPs) HSP27, HSP70, and HSP90 and the activator of 90-kDa HSP ATPase homolog 1 (AHA1) are all stress-responsive proteins[23,24] that are known to be involved in the processing of CFTR.[21] HSP90 levels increase during stress in order to guard against misfolded proteins,[25] and AHA1 is an activator of HSP90 ATPase.[26] HSP70 is upregulated in cancer cells and is associated with a negative outcome.[27,28] In addition, HSP70 and HSP90, in combination with AHA1, inhibit the surface expression of CF mutant F508-del CFTR, clearly indicating their role in CFTR trafficking from the endoplasmic reticulum (ER) to the plasma membrane.[21] HSP27 (HSPB1), a member of the small HSP family, is thought to guard against protein aggregation during stress.[29] We have shown previously that HSP27, HSP70, and HSP90 are all elevated in cystic kidneys derived from mice lacking PC1 when compared with wild-type (WT) control animals. One question to be addressed is whether these same HSPs are involved in ARPKD.

CFTR Correctors and Potentiators

The corrector VX-809 (lumacaftor) was developed to rescue the F508-del CFTR mutant.[30] Because CFTR is present in cysts,[31] many researchers have suggested that CFTR inhibitors might be therapeutic in reducing fluid secretion.[32–36] However, we have shown previously that the CFTR corrector VX-809 can reduce cysts[37] in mouse- and cell-based models of ADPKD. In the cysts, CFTR is present at the apical membrane, which is why CFTR-based inhibitors can reduce cyst growth to some extent. Surprisingly, however, when VX-809 is applied, CFTR moves to the basolateral membrane and promotes an absorptive phenotype, which then shrinks the cysts. The overall goal of our study here is to understand the role of CFTR in ARPKD and

Most current article

uncover therapeutic targets for pharmacological strategies to treat ARPKD.

Results

Pkhd1[del4/del4] Cholangiocytes

To begin to identify strategies to treat ARPKD, we conducted experiments in WT and *Pkhd1*[del4/del4] cholangiocytes (hereafter referred to as *del4*), obtained from the Yale O'Brien Center and isolated as described in the Materials and Methods. The cholangiocytes were isolated from WT and *Pkhd1*[del4/del4] mice, the latter a model of ARPKD.[38] These mice, with a disruption in exon 4 of the *Pkhd1* gene, display intrahepatic bile duct proliferation, progressive liver cyst formation, and periportal fibrosis, along with pancreatic cysts and splenomegaly.

To begin to characterize these mutant cholangiocytes, we measured their steady-state levels of FPC. Figure 1*A* and *B* shows that the *del4* cholangiocytes have levels of FPC substantially lower than those observed in WT cholangiocytes. Detectable FPC protein in the *del4*- cholangiocytes is expected because the out-of-frame deletion of exon 4 uncovers a cryptic splice site that creates an in-frame, hypomorphic transcript[38] expressing a protein with a 66-amino-acid deletion. Application of 10 uM of VX-809 does not change FPC expression. It is unlikely that this residual protein is functional, given that the mice bearing this mutant have liver disease reminiscent of human pathology.

CFTR Protein Expression

As mentioned previously, the roles of CFTR in ARPKD are unclear. To examine the expression of CFTR in cholangiocytes, we performed Western blotting (Figure 1*C* and *D*). We detected a sharp drop in CFTR in *del4* cholangiocytes when compared with WT cells. CFTR is well known to exist in an immature, core-glycosylated form that resides primarily in the ER (the B band) and as a mature, fully glycosylated form (the C band), see Cheng et al.[39] Thus, it is important to note that in *del4* cholangiocytes, the mature fully glycosylated form of CFTR is absent. The processing induced by correctors usually involves the conversion of B bands to C bands as the processing is restored by the corrector[30]; however, the application of VX-809 does increase CFTR protein levels, but the mature form of CFTR is not fully restored.

Sox9 Expression

Sox9 is present in ductal epithelia such as cholangiocytes.[40] Thus, to verify that the cells were cholangiocytes, we assayed the cells for the presence of Sox9. Figure 1*E–H* shows that Sox9 is expressed in both WT and *del4* cholangiocytes. We saw no change in Sox9 either in normal, *del4* cholangiocytes or the latter treated with VX-809.

Reducing the Cysts

As mentioned previously, the *Pkhd1*[del4/del4] mice develop multiple liver cysts with age.[38] To study this phenomenon, we grew WT and *del4* cholangiocytes in 3-dimensional (3D) culture. Figure 2 shows that cysts developed in 3D culture from the *del4* cholangiocytes but cells from WT animals remain as small clumps. In ADPKD resulting from a malfunction of either PC1 or PC2, cyst growth is accelerated by adenosine 3′,5′-cyclic monophosphate (cAMP).[41] Similarly, cyst growth in *del4* cholangiocytes was accelerated by forskolin, which stimulates cAMP.[42] Please note that 2 different
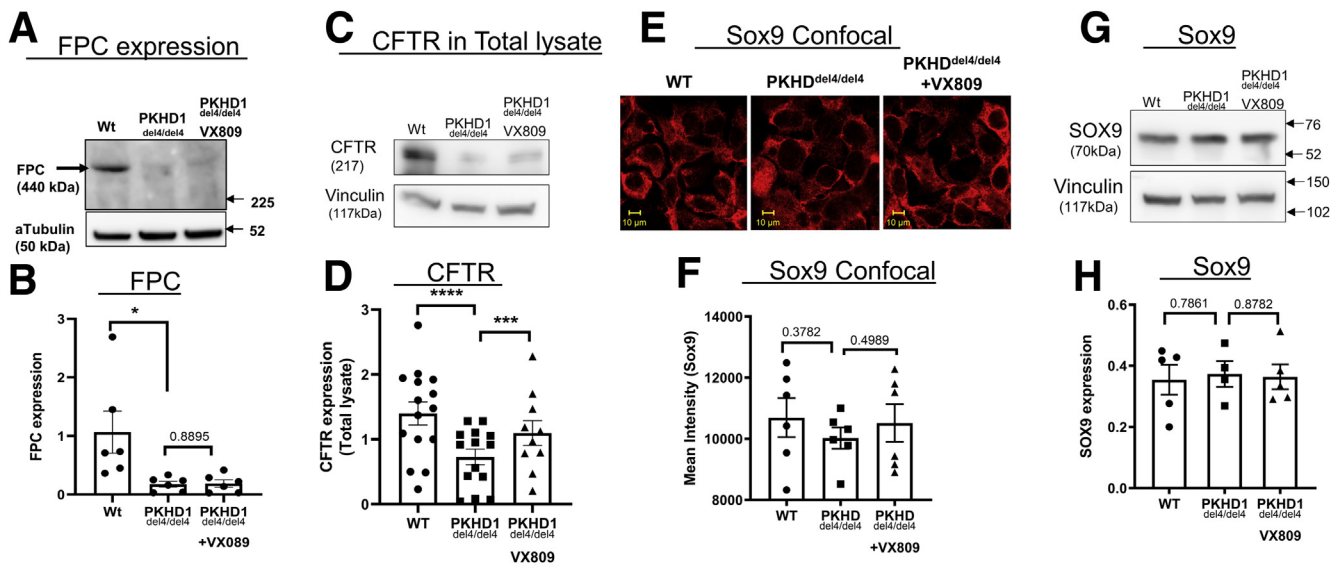

Figure 1. FPC in *Pkhd1*[del4/del4] (*del4*) cholangiocytes. (*A*) Western blotting for FPC. Please note that *del4* cells have substantially less FPC. Antibody was obtained from the Baltimore PKD Center. α-Tubulin was used as the loading control. (*B*) Summary. Reduced CFTR in *del4* cholangiocytes. (*C*) Western blot showing CFTR. (*D*) Summary. (*E*, *F*) Sox9: WT, *del4*, and VX-809–treated *del4* cholangiocytes stained for Sox9 (red), expressed as mean intensity. (*G*) Western blotting for Sox9. (*H*) Summary data. Number of Western blot experiments represented in the figure (dots) are from independent 10-cm dishes of cultured cells. Student's *t* test. *$P < .05$; ***$P < .001$; ****$P < .0001$.
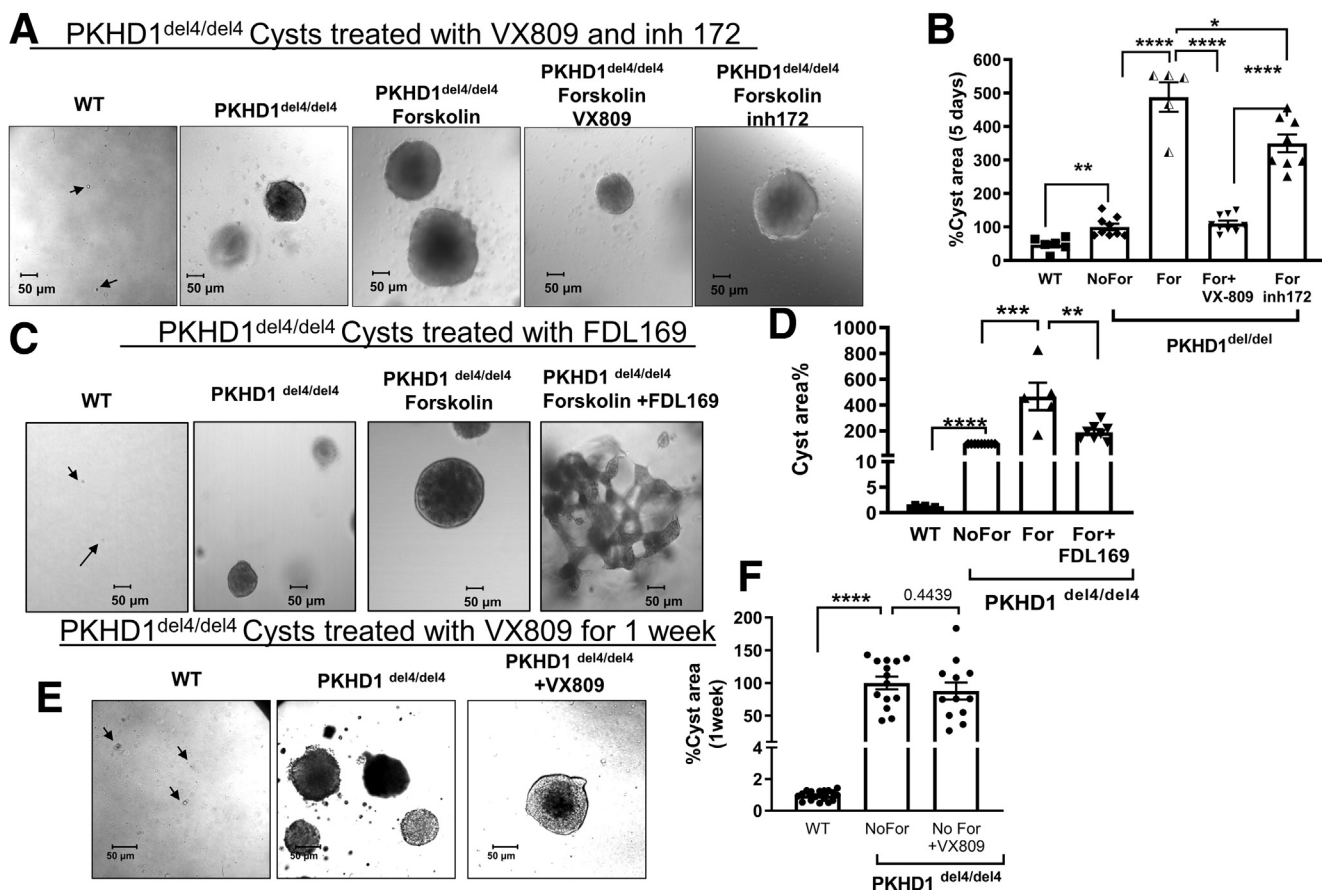
Figure 2. VX-809–mediated reduction in cyst formation. WT and *del4* cholangiocytes were grown on Matrigel and monitored for 1 week. Cholangiocytes treated with (*A*, *B*) VX-809 or (*C*, *D*) FDL169. A smaller total cystic area was observed after treatment with either corrector. Cysts were induced with forskolin (For) (10 μM) for 24 hours on day 6. Arrows indicate WT cells. (*E*, *F*) Cholangiocytes were treated with VX-809 in the absence of forskolin. Cyst growth was monitored every other day. Cysts were treated with VX-809 (10 μM) for 10 days, with the medium was replaced every 48 hours. Number of cysts measured are represented in the figure as dots. Student's *t* test. *$P < .05$; **$P < .01$; ***$P < .001$; ****$P < .0001$.

CFTR correctors, VX-809 and FDL169,[43] both reduced cyst growth even in the presence of forskolin stimulation. When we used the CFTR inhibitor 172,[35] cyst growth was also reduced but to nowhere near the extent seen for VX-809. These data suggest that CFTR modulators such as VX-809 and FDL169 are likely to have greater potential than CFTR inhibitors for use as therapeutics for ARPKD. VX-809 does not have an effect on cyst growth in the absence of forskolin (Figure 1*E* and *F*).

Location of CFTR in Cholangiocytes

Next, we determined the location of CFTR in cysts (Figure 3*A*–*D*). Consistent with its role in fluid secretion in the bile duct,[44] CFTR colocalizes with the apical marker wheat germ agglutinin (WGA) in WT cholangiocytes. In *del4* cholangiocytes there is a reduction in colocalization of CFTR with the apical and most dramatically with the basolateral membrane. VX-809 increased the colocalization of CFTR with both the apical and basolateral membrane markers. To take this one step forward, we determined the location of CFTR in cholangiocytes grown on permeable supports using confocal microscopy (Figure 3*E*–*J*). Note

that CFTR colocalized with the apical membrane marker WGA in WT and *del4* cholangiocytes. Importantly, the colocalization was increased in the presence of VX-809. Interestingly CFTR also colocalizes with the basolateral membrane marker, Na$^+$/K$^+$ ATPase, but less so. VX-809 caused an increase in colocalization with the basolateral membrane marker Na$^+$/K$^+$ ATPase in both WT and *del4* cholangiocytes.

HSPs Play an Important Role in ARPKD

A myriad of proteins forming a proteostatic network are involved in the processing and trafficking of CFTR. To delineate the role of HSPs in ARPKD, we measured their protein expression by Western blotting. The absence of FPC had a profound effect on the HSPs, causing a large reduction in the protein levels of HSP27 and dramatic increases in HSP90 and HSP70 (Figure 4). The next question we asked was whether these changes affected cyst growth and the localization of CFTR.

To evaluate this question, we first focused on HSP27. To determine whether low levels of HSP27 affected cyst growth, we transfected additional HSP27 into *del4* cholangiocytes.
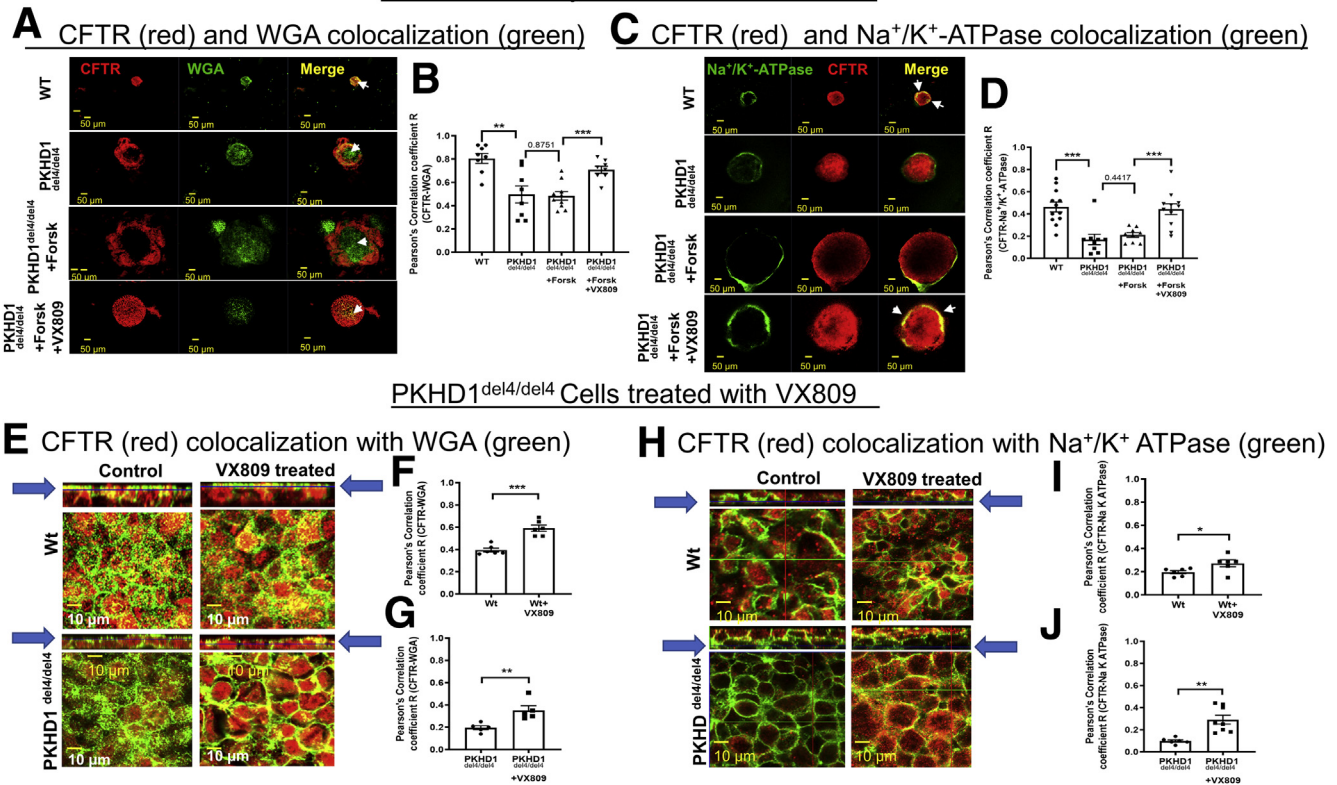
Figure 3. Colocalization of CFTR with (*A, B*) WGA and (*C, D*) Na^+/K^+ ATPase in VX-809–treated WT or mutant (*Pkhd1$^{del4/del4}$*) cholangiocyte cysts. WT or mutant *del4* cholangiocytes were grown on Matrigel. For immunostaining, 3D cultures were treated with collagenase 1 to improve the permeability through the Matrigel and then fixed with 4% PFA. Double-labeled immunofluorescence images stained for CFTR (red), (*A*) WGA or (*C*) Na^+/K^+ ATPase (green), and the merged image. Yellow denotes colocalization. (*B, D*) Pearson's correlation coefficient (R). Scale bar = 50 μm. White arrows indicate the colocalization of CFTR and WGA or CFTR and Na^+/K^+ ATPase at the apical or basolateral regions of the cells, respectively. Each set of data is from multiple regions of 7-8 individual cysts. **CFTR expression and localization**: Localization of CFTR to (*E*) apical vs (*H*) basolateral membranes. (*E–G*) CFTR (red) and WGA (green) in WT or *del4* cholangiocytes treated with VX-809 (10 μM). Pearson's correlation coefficient R. (*H–J*) CFTR (red) and Na^+/K^+ ATPase (green) in WT or d*el4* cholangiocytes treated with VX-809 (10 μM). Pearson's correlation coefficient R. Cells were grown on Transwell membranes. Strips = Z-stacks of confocal images acquired at 0.4 μm using a 63× oil objective. Arrows point to the Z-stack image corresponding to the accompanying figure immediately below. In this figure and all subsequent confocal images, 1 Z-stack plane is shown. As noted by the arrows, Z-stack planes for apical localization were selected toward the apical pole of the cells. In contrast, Z-stack planes for basolateral localization were selected toward the basolateral pole of the cells. Scale bar = 10 μm. All data are expressed as mean ± SEM. *P* values were determined by Student's *t* test. For quantification of colocalization, 2–3 random areas were measured along a single z-plane as depicted by the arrows, from 3 individual slides for each group. *$P <$ .05; **$P <$ .01; ***$P <$ .001.

Transfecting additional HSP27 into *del4* cholangiocytes (see Figure 5*A* and *B*) to restore the protein levels to near WT values induced a profound reduction in cyst growth (Figure 5*C* and *D*). Note that similar to VX-809, transfecting additional HSP27 caused an increase in colocalization with the apical marker WGA and the basolateral membrane marker Na^+/K^+ ATPase in *del4* cholangiocytes toward WT values (Figure 5*E–H*).

Next, we focused on HSP90. Because HSP90 expression is elevated in *del4* cholangiocytes, we silenced HSP90 using small interfering RNA to reduce its protein levels (Figure 6*A* and *B*). Reducing HSP90 protein levels using small interfering RNA had a profound effect on cyst size even in the presence of forskolin (Figure 6*C* and *D*).

We also applied the HSP90 inhibitor KW-2478[45] to reduce HSP90 protein and activity. Note that application of KW-2478 reduced HSP90 protein levels (Figure 7*A* and *B*) and reduced cyst growth (Figure 7*C* and *D*). Note that similar to VX-809, the HSP90 inhibitor KW-2478 caused an increase in colocalization of CFTR with the apical marker WGA and the basolateral membrane marker Na^+/K^+ ATPase in *del4* cholangiocytes toward WT values (Figure 7*E–H*).

Finally, we focused on HSP70. Because HSP70 expression is elevated in *del4* cholangiocytes, we applied the HSP70 inhibitor, VER155008,[46] which did not affect the steady state levels of HSP70 (Figure 8*A* and *B*). Similar to HSP90, the HSP70 inhibitor reduced cyst growth (Figure 8*C* and *D*). Note that similar to VX-809, the HSP70 inhibitor caused an increase in colocalization of CFTR with the apical marker WGA and the basolateral membrane marker Na^+/K^+ ATPase in *del4* cholangiocytes toward WT values (Figure 8*E–H*).

A Heat shock protein expression

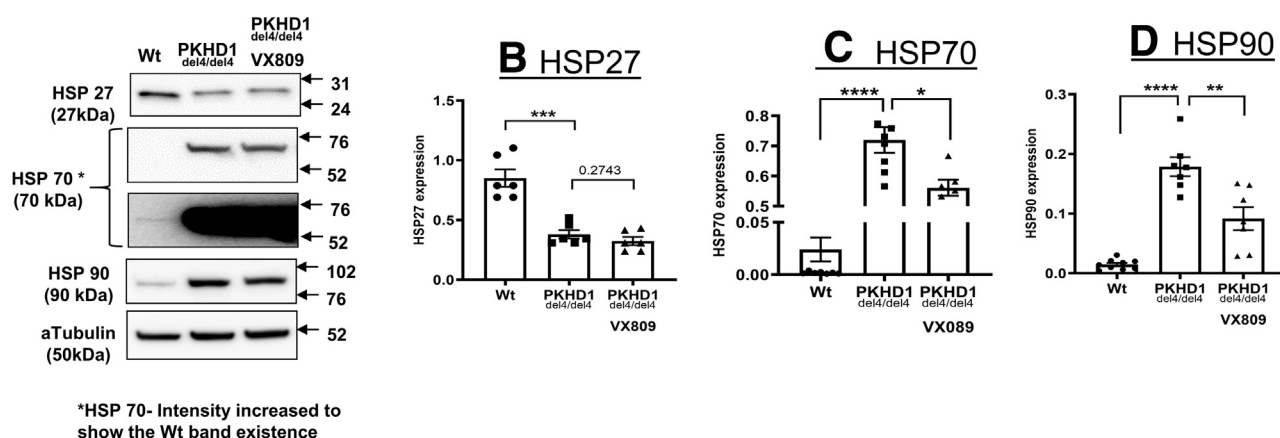*HSP 70- Intensity increased to
show the Wt band existence

Figure 4. ERAD protein expression in ARPKD cells. (*A*) Western blot of HSP27, HSP70, and HSP90 in WT or *del4* chol-angiocytes and *del4* cells treated with VX-809 *(10 μM)*. α-tubulin was used as the loading control. (*B–D*) Summary data. All data are expressed as mean ± SEM. *P* values were determined by Student's *t* test. Please note that the same gel for HSP70 is presented at 2 different exposure times. Number of Western blot experiments represented in the figure (dots) are from in-dependent 10-cm dishes of cultured cells. *$P < .05$; **$P < .01$; ***$P < .001$; ****$P < .0001$.

Thus, in their entirety, our data show that the HSPs play an important role in fueling cyst growth in ARPKD and altering the localization of CFTR.

Discussion

Defective Processing of CFTR

We show here that FPC malfunction in cholangiocytes affects several cellular processes that have a profound impact on the trafficking and processing of proteins such as CFTR. We observed that CFTR is expressed in the chol-angiocytes at a much lower level in *del4* cholangiocytes than in WT cells, demonstrating that in the absence of FPC, the steady-state levels of CFTR fall. This result is interesting, given that Nakanishi et al[14] showed that creating a double knockout of CFTR and FPC makes the phenotype of the mouse worse than that of a mouse bearing only a mutant FPC gene. These data regarding the double-knockout mice, together with our observed reduction in CFTR levels in *del4* cholangiocytes, suggests that a deficit in CFTR expression contributes to the pathologies noted in ARPKD. Interest-ingly, the reduction in CFTR protein in *del4* cholangiocytes was associated with an increase in the presence of the immature, lower-molecular-weight B-band of CFTR. CFTR is well characterized with regard to its processing and exit from the ER, and the presence of the also B-band is well known to indicate arrested processing and trafficking from the ER.[47] Thus, the lower levels of CFTR are suggestive of defective processing in *del4* cholangiocytes.

ER-Associated Protein Degradation

Because we noted changes in CFTR that point to its misprocessing, we decided to determine whether key ER–associated degradation (ERAD) proteins, including HSPs,[48] are altered in the *del4* cholangiocytes. We were surprised to detect a drop in HSP27 because we have

previously shown that when PC1 malfunctions, HSP27 is upregulated.[49] A reduction in HSP27 levels clearly plays a role in this process because transfecting additional HSP27 reduces cyst growth. HSP27 plays many roles in cells, ranging from protecting the cells from misfolded proteins to regulating actin stability and inflammation.[50] Interestingly, both upregulation and downregulation of HSP27 levels are associated with many diseases.[50] For example, in certain cancers such as bladder cancer, HSP27 is upregulated to prevent aggregation of proteins. In this instance, reducing HSP27 reduces cancer progression.[51] At the opposite extreme, in retinopathy, high glucose in retinal capillary cells causes a downregulation of HSP27 induced by proin-flammatory cytokines that stimulates apoptosis, thereby potentially contributing to the retinopathy.[52] In our expe-rience, the most common mutation in CFTR, F508-del, in-creases HSP27 in airway cells, most likely protecting them from the misfolded F508-del protein.[53] On the other hand, in some mutant forms of ABCA4 associated with Stargardt disease, HSP27 levels are downregulated.[54] Recently, we have shown that a reduction in HSP27 is one of the out-comes of *Clostridium difficile* infection.[55] These polar dif-ferences in disease-associated changes in HSP27 reflect the different pathological outcomes associated with the disease process. For example, in cancer as well as ADPKD, high HSP27 levels may protect the dividing cells from unfolded proteins and apoptosis, allowing them to grow pathologi-cally, whereas in *C. difficile*, a reduction in HSP27 is asso-ciated with a reduction in the epithelial barrier in infected GI tract cells that leads to inflammatory diarrhea.

HSP27 is known to bind to actin and increase the sta-bility of F-actin (filamentous actin),[56] 1 of the 2 forms of actin in cells. The dynamic interchange between the 2 actin forms, F-actin and G-actin (globular actin), is critical for the proper functioning of the cellular cytoskeleton.[56] A reduc-tion in HSP27 has been shown to have a deleterious effect
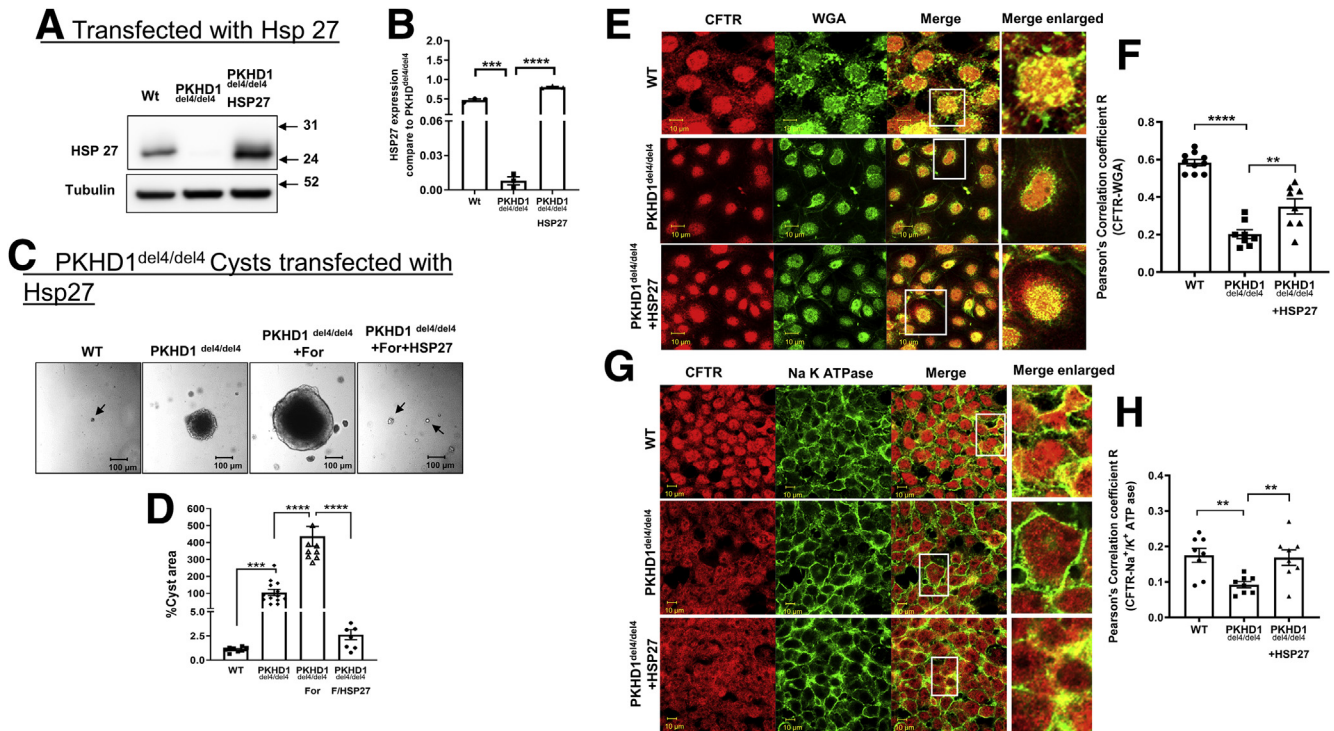
Figure 5. Maneuvers that reduce cysts increasing HSP27. WT, *del4* cholangiocytes, and *del4* cholangiocytes transfected with HSP27. (*A, B*) Western blot confirming HSP27 transfection. α-Tubulin was used as the loading control. WT and *del4* cholangiocytes were grown on Matrigel and monitored for 1 week. (*C, D*) Significant reduction in cyst area as compared with WT cholangiocytes was observed in HSP27-transfected cholangiocytes. Localization of CFTR to (*E, F*) apical vs (*G, H*) basolateral membranes. (*F*) CFTR (red) and WGA (green) in WT or *del4* cholangiocytes treated with VX-809 (10 μM). Pearson's correlation coefficient R. (*G, H*) CFTR (red) and Na$^+$/K$^+$ ATPase (green) in WT or *Del4* cholangiocytes. Cells were grown on Transwell membranes. Z-stacks of confocal images acquired at 0.4 μm using a 63$\times$ oil objective but representative images of the apical location for WGA vs the more basolateral image for Na$^+$/K$^+$ ATPase. A portion of the image demarcated by a white box was enlarged on the right. Scale bar = 10 μm. All data are expressed as mean $\pm$ SEM. *P* values were determined by Student's *t* test. For quantification of colocalization, 2–3 random areas were measured along a single z-plane as depicted by the arrows, from 3 individual slides for each group. Number of cysts represented in the figure (dots) are from individual cysts. *P < .05; **P < .01; ***P < .001; ****P < .0001.

on cells, particularly with regard to disrupting actin dynamics.[56] The phenotype in ARPKD differs from ADPKD in the development of ductal plate abnormalities and fusiform dilation in the collecting ducts.[9] It is interesting that the cortical location of the actin cytoskeleton observed in normal inner medullary collecting duct cells is disrupted by silencing *Pkhd1*, which in turn leads to an epithelial-to-mesenchymal transition,[57] perhaps as a result of enhanced RhoA levels in kidney cells.

Here, we have also demonstrated that HSP90 and HSP70 are upregulated in cholangiocytes. Furthermore, we have shown that reducing HSP90, either by silencing its transcription or by the use of an inhibitor, reduces cyst growth. This result is consistent with our data showing that CFTR protein levels are reduced in *del4* cholangiocytes. Given that HSP70 and 90 are known to play a role in the processing of CFTR[21], these data demonstrate clearly the role of these proteins in CFTR trafficking from the ER to the plasma membrane.

Along these lines, HSP90 is overactive in ADPKD cells, and a reduction in its function decreases cyst growth.[58,59] Seeger-Nukpezah et al[59] showed that application of the

small molecule inhibitor STA-2842 over a 10-week period not only inhibits the initial formation of cysts, but also slows the progression of preexisting cysts, not unlike our observations here. Thus, elevations in HSP90 and HSP70 appear to be common to both ARPKD and ADPKD.

Role in CFTR trafficking

CFTR is normally found in the apical membrane of cholangiocytes, where it participates in fluid secretion.[60] Consistent with this localization, we found that in WT cholangiocytes, CFTR colocalizes principally with apical membrane markers. CFTR also colocalizes with the basolateral membrane marker Na$^+$/K$^+$ ATPase, albeit less strongly. It is known that in secretory epithelia, newly processed CFTR first traffics to the basolateral membrane and then is transcytosed to the apical membrane.[61] Thus, it is not unusual to detect CFTR colocalization within the basolateral membrane. One can readily see that in *del4* cholangiocytes, the colocalization of CFTR with the basolateral marker is reduced, likely contributing to cyst formation in a manner similar to that in ADPKD.[31] VX-809
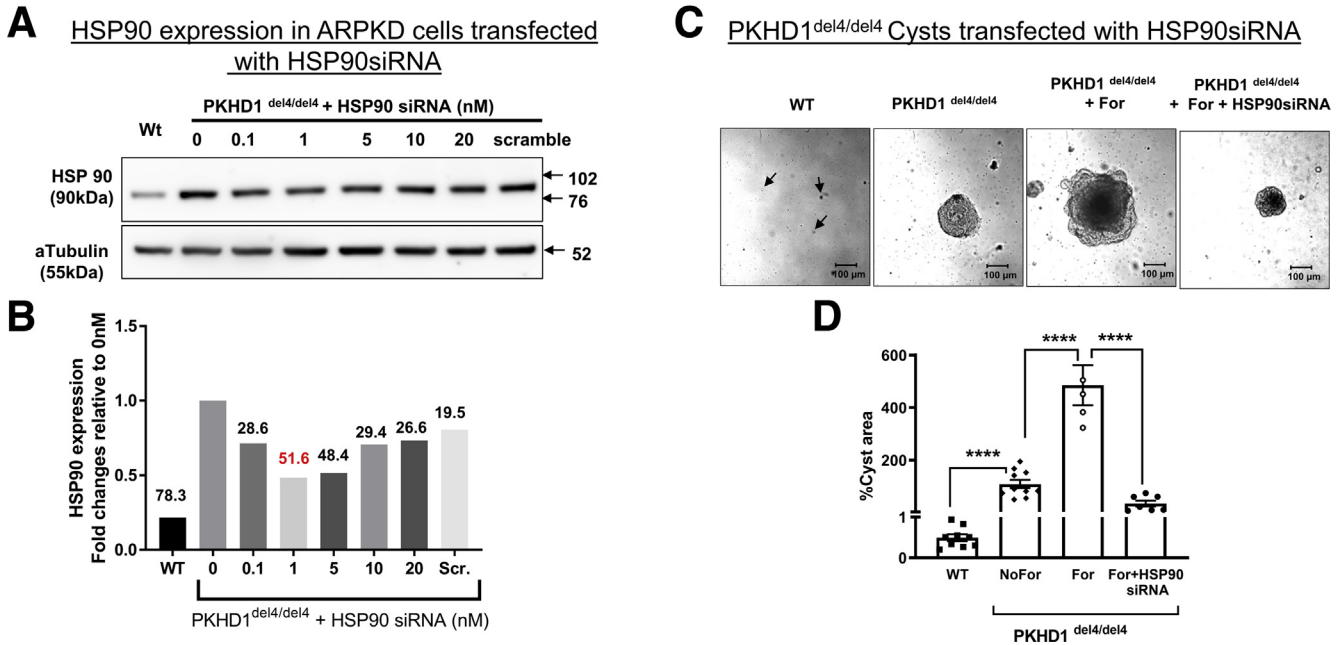
A HSP90 expression in ARPKD cells transfected with HSP90siRNA

B

C PKHD1del4/del4 Cysts transfected with HSP90siRNA

D

Figure 6. Silencing HSP90. (*A*, *B*) Western blots showing optimization of HSP90 silencing. WT and *del4* cholangiocytes were grown on Matrigel and monitored for 1 week. (*C*, *D*) Cyst growth is inhibited by silencing HSP90. All data are expressed as mean ± SEM. *P* values were determined by Student's *t* test. Number of cysts represented in the figure (dots) are from individual cysts. Number of Western blot experiments represented in the figure (dots) are from independent 10-cm dishes of cultured cells. ****$P < .0001$. siRNA, small interfering RNA.

treatment increased CFTR expression in *del4* cholangiocytes at the apical and basolateral membranes. We have previously demonstrated a similar pattern in PC1-null cells derived from the kidney.[37] In that study, we showed that the trafficking and function of transporters involved in Na$^+$ absorption, such as NHE3 and ENaC, are also restored by VX-809, reversing the cyst phenotype from secretion to absorption.

CFTR Modulators

We have shown here that the CFTR corrector VX-809, which was designed to rescue F508-del CFTR, reduces cyst growth in *del4* cholangiocytes essentially as it does in PC1-deficient proximal tubule cells and in a PC1-null model of ADPKD.[37,49] The overarching similarity in these scenarios is that VX-809 increases the localization of CFTR in the basolateral membrane. We suggested in our previous work that this movement of CFTR to the basolateral membrane reduces the phenotype of the cysts from secretory to absorptive.[37] VX-809 does not have any effect on the cysts in the absence of forskolin. This is not surprising because CFTR is not the only channel driving fluid secretion in the cysts.[31] For example, the calcium activated chloride channel, Anoctamin 1 also supports cyst growth, particularly in response to signal transduction mechanisms which increase Ca^{2+}.[62] Moreover, VX-809 increases the processing and trafficking of CFTR but does not active it.[30] CFTR is activated though protein kinase A via cAMP.[63] Thus, in our scenario, VX-809 moves CFTR to the basolateral membrane and then forskolin activates and increase in cAMP and subsequent increase in active protein kinase A, thereby reducing the cysts.

It is also informative to determine what VX-809 fails to rescue. Although our transfection experiments show that HSP27 plays a role in cyst growth, VX-809 does not restore HSP27 toward WT values, indicating that VX-809 and HSP27 reduce cyst growth by different mechanisms.

Conclusion

We found that a deficit of FPC in cholangiocytes leads to a reduction in CFTR and profound changes in an ensemble of ERAD proteins that are known to play a role in CFTR processing such as HSP27, HSP90, and HSP70.[64] VX-809 also reduces ERAD proteins, which are implicated in retaining CFTR in the ER and thus promoting the trafficking of CFTR to the basolateral membrane, where it can participate in reducing cysts. These data suggest that CFTR correctors could be useful and therapeutics for ARPKD. Given that they are already approved for use in humans,[65] they can be fast-tracked for clinical use for ADPKD.

Materials and Methods
Reagents

Forskolin (#11018) was purchased from Sigma-Aldrich (St Louis, MO); VX-809 (#S1565) and FDL169 (#S8795) were purchased from Selleck Chemicals (Houston, TX); HSP27 (SC13132), HSP70 (SC66048) antibodies were purchased from Santa Cruz Biotechnology (Dallas, TX); Sox9
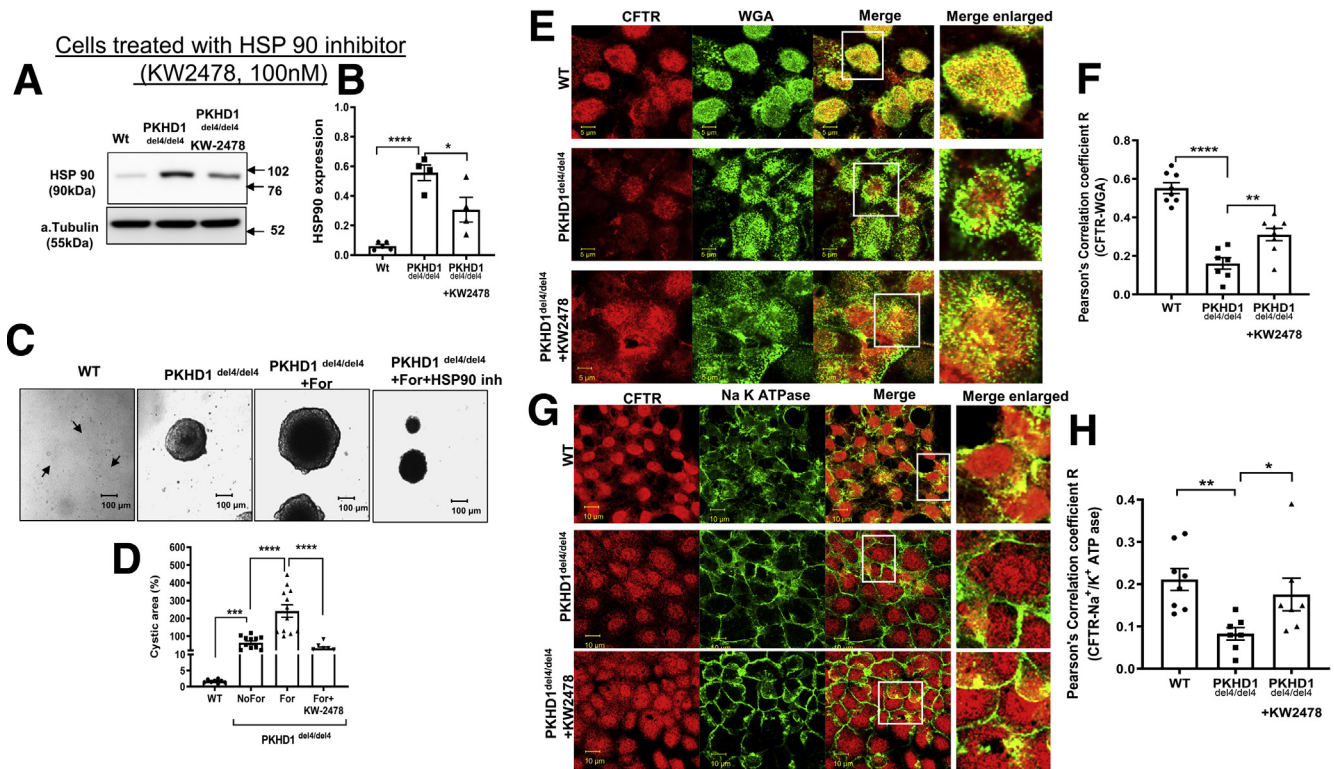
Figure 7. Maneuvers that reduce cysts inhibiting HSP90. (*A*, *B*) Western blot of WT and *del4* cholangiocytes treated with KW-2478. WT and *del4* cholangiocytes were grown on Matrigel and monitored for 1 week. (*C*, *D*) A significant difference from WT in cyst area was observed in HSP90 inhibitor treated cholangiocytes. Localization of CFTR to (*E*, *F*) apical vs (*G*, *H*) basolateral membranes. CFTR (red) and WGA (green) in WT or *del4* cholangiocytes treated with VX-809 (10 μM). (*F*, *H*) Pearson's correlation coefficient R. (G, H) CFTR (red) and Na$^+$/K$^+$ ATPase (green) in WT or *Del4* cholangiocytes. Cells were grown on Transwell membranes. Z-stacks of confocal images acquired at 0.4 μm using a 63$\times$ oil objective but representative images of the apical location for WGA vs. the more basolateral image for Na$^+$/K$^+$ ATPase. A portion of the image demarcated by a white box was enlarged on the right. Scale bar = 10 μm. All data are expressed as mean $\pm$ SEM. *P* values were determined by Student's *t* test. For quantification of colocalization, 2–3 random areas were measured along a single z-plane as depicted by the arrows, from 3 individual slides for each group. Number of cysts represented in the figure (dots) are from 3 independent experiments. Number of Western blot experiments represented in the figure (dots) are from independent 10 cm dishes of cultured cells. Number of Western blot experiments represented in the figure (dots) are from independent 10 cm dishes of cultured cells. *$P < .05$; **$P < .01$; ***$P < .001$; ****$P < .0001$.

(ab185230) and Na$^+$/K$^+$ ATPase (#ab76020) antibodies were purchased from Abcam (Cambridge, United Kingdom); WGA (#W11261) was purchased from Invitrogen (Waltham, MA); and HSP90 (ADI-SPA-830F) antibody was purchased from Enzo Life Sciences (Farmingdale, NY).

Isolation of Cholangiocytes From WT-C57Bl/6 and Pkhd1$^{del4-/del4}$ Mice

To create the cholangiocyte cultures, WT-*C57Bl/6* and *Pkhd1$^{del/4/del4}$* mice[66] were crossed with mice transgenic for the Sv40 large T antigen (strain name SV40 T-antigen, JAX strain #002233). Segments of intrahepatic bile ducts were microdissected from livers that had been perfused via the portal vein with molten agarose containing toluidine blue to mark the veins. The liver parenchyma was stripped until the biliary tree was identified, and the bile duct units were seeded onto rat type I collagen-coated plates. The cells were cultured under non-permissive conditions in the following mixed medium: Dulbecco's modified Eagle medium/F12

with 5% fetal bovine serum, 10-μL/mL insulin-transferrin-selenium, 3.4-μg/mL tri-iodothryrodine, and 50,000 units of penicillin/streptomycin under humidified conditions at 37°C in 5% CO$_2$. After 1 week, the cells were cultured under permissive conditions in the presence of 10 units of interferon-γ at 33°C in 5% CO$_2$. When confluent, the cells were passaged by digesting the collagen slab below the cells (60 minutes; 37°C; Dulbecco's modified Eagle medium/F12 with 2-mg/mL dispase and 1-mg/mL collagenase type 11), then washed twice in phosphate-buffered saline (PBS) and plated onto collagen-coated support systems. Clonal cell lines were generated by single-cell isolation. For experimental use, the cells were differentiated for 10 days at 37°C without interferon-γ.

In Vitro Cystogenesis

To induce differentiation, cells were kept at 37°C for at least 6 days without interferon-γ. After 1 week, the cells were used for 3D culture or other experiments. Growth
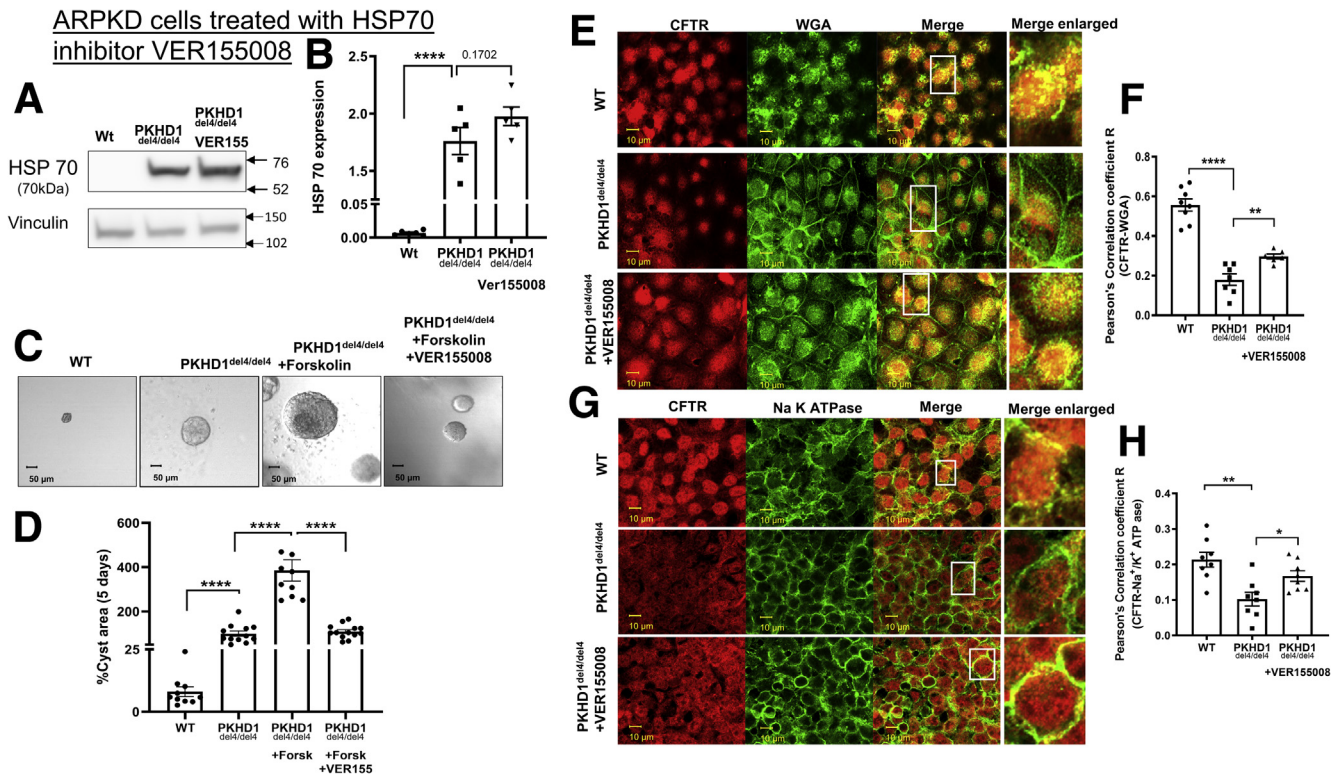
Figure 8. Maneuvers that reduce cysts inhibiting HSP70. (*A*, *B*) Western blot of WT and *del4* cholangiocytes treated with VER155008. WT and *del4* cholangiocytes were grown on Matrigel and monitored for 1 week. (*C*, *D*) Cystic cells were treated with HSP70 inhibitor (VER155008). A significant difference from WT in cyst area was observed in HSP70 inhibitor treated cholangiocytes. Localization of CFTR to (*E*, *F*) apical vs (*G*, *H*) basolateral membranes. CFTR (red) and WGA (green) in WT or *del4* cholangiocytes treated with VER155008 (10 μM). Pearson's correlation coefficient R. (*F*) CFTR (red) and (*H*) Na$^+$/K$^+$ ATPase (green) in WT or *del4* cholangiocytes. Cells were grown on Transwell membranes. Z-stacks of confocal images acquired at 0.4 μm using a 63$\times$ oil objective but representative images of the apical location for WGA vs. the more basolateral image for Na$^+$/K$^+$ ATPase. A portion of the image demarcated by a white box was enlarged on the right. Scale bar = 10 μm. All data are expressed as mean $\pm$ SEM. *P* values were determined by Student's *t* test. For quantification of colocalization, 2–3 random areas were measured along a single z-plane as depicted by the arrows, from 3 individual slides for each group. Number of Western blot experiments represented in the figure (dots) are from independent 10-cm dishes of cultured cells. Number of cysts represented in the figure (dots) are from individual cysts. *$P < .05$; **$P < .01$; ***$P < .001$; ****$P < .0001$.

factor–reduced Matrigel #354230 (Corning, Corning, NY) was used here, and cell dilutions were prepared so that there were approximately 6000 cells in 25 μL of medium; 25 μL of cell preparation was mixed with 50 μL of Matrigel, see Yanda et al.[67] Pictures were taken with a Zeiss Axio microscope (Zeiss, Oberkochen, Germany). Cystic areas were analyzed with ImageJ 1.50i (provided by the National Institutes of Health, Bethesda, MD).

Immunofluorescent Staining

WT or *del4* cells were grown on Transwell membranes of a 6-well plate for 4 days. Following the confluence of cells each Transwell membrane apparatus was transferred to a new plate and membranes were washed with PBS for 3 times. Cells on membranes were fixed with 4% formaldehyde. Cells were then washed 3 times with PBS and blocked, permeabilized with PBS containing 1% bovine serum albumin, 0.2% Triton X-100. Following blocking, membranes were incubated with primary antibodies for overnight at 4°C and then processed for secondary antibody. Following antibody staining and washings, membranes were mounted

on glass slides using Fluoro-gel (EMS#17985-10) and covered with coverslips. Images were captured using Zeiss LSM 880 confocal microscope.

Western Blot

WT or *del4* cells were harvested and solubilized in NP40 lysis buffer (1% NP40, 50-mM Tris HC, 150-mM NaCl), containing protease inhibitor cocktail (catalog# 78438; Thermo Fisher Scientific, Waltham, MA). Lysates were rotated for 20 minutes at 4°C. Following the lysis samples were centrifuged at 14,000 *g* for 15 minutes at 4°C to pellet the insoluble material. Supernatant was carefully transferred to a new clean tube for protein concentration measurements. Supernatants were mixed with 2X Laemmli sample buffer (#1610737; Bio-Rad, Hercules, CA). Each 50 μg of protein sample was subjected to sodium dodecyl sulfate polyacrylamide gel electrophoresis using 4%–15% protein TGX precast gel (#4561084; Bio-Rad). Proteins were transferred onto polyvinylidene difluoride membrane (#1704157; Bio-Rad) using Bio-Rad turbo transfer system, followed by blocking the membrane in 5% non-fat milk in

TBST for 1hr at room temperature. Membranes were washed twice with TBST (tris-buffered saline with 0.05% tween20 and incubated with primary antibody (1:1000) diluted in blocking buffer for overnight at 4°C. Following the primary antibody incubation, membranes were washed 3 times and incubated with horseradish peroxidase conjugated secondary antibody for 1h at room temperature followed by washing with TBST for 3 times. The protein of interest was detected using Enhanced chemiluminescence (SuperSignal West Dura Extended Duration Substrate, catalog no. 34075; Thermo Fisher Scientific) reagent. The chemiluminescent signal on the polyvinylidene difluoride membrane was directly captured using Amersham Imager 600 (Amersham, Amersham, United Kingdom) equipped with a cooled CCD camera. ImageQuant TL 8.1 software (Cytiva, Marlborough, MA) was used for quantification of the bands.

Statistics

Averages ± SEM are given for all data. Data were analyzed by Student's *t* test. Brackets indicate the compared values. The number of independent experiments is represented in each figure as a dots. The *del4* and control cells originated each from 1 animal. Experiments on cultured cells were conducted on independent cultures of cells. For quantification of colocalization, 2–3 random areas were measured along a single z-plane from 3 individual slides for each group. For cysts, n indicates the number of individual cysts. All experiments were replicated until statistically significant at $P < .05$. Statistical significance was determined by Student's *t* test. All experiments were unblinded. All data points are depicted in the figures.

References

1. Ward CJ, Hogan MC, Rossetti S, Walker D, Sneddon T, Wang X, Kubly V, Cunningham JM, Bacallao R, Ishibashi M, Milliner DS, Torres VE, Harris PC. The gene mutated in autosomal recessive polycystic kidney disease encodes a large, receptor-like protein. Nat Genet 2002;30:259–269.
2. Nagasawa Y, Matthiesen S, Onuchic LF, Hou X, Bergmann C, Esquivel E, Senderek J, Ren Z, Zeltner R, Furu L, Avner E, Moser M, Somlo S, Guay-Woodford L, Buttner R, Zerres K, Germino GG. Identification and characterization of Pkhd1, the mouse orthologue of the human ARPKD gene. J Am Soc Nephrol 2002;13:2246–2258.
3. Sweeney WE Jr, Avner ED. Molecular and cellular pathophysiology of autosomal recessive polycystic kidney disease (ARPKD). Cell Tissue Res 2006;326:671–685.
4. Zerres K, Mucher G, Becker J, Steinkamm C, Rudnik-Schoneborn S, Heikkila P, Rapola J, Salonen R, Germino GG, Onuchic L, Somlo S, Avner ED, Harman LA, Stockwin JM, Guay-Woodford LM. Prenatal diagnosis of autosomal recessive polycystic kidney disease (ARPKD): molecular genetics, clinical experience, and fetal morphology. Am J Med Genet 1998;76:137–144.
5. Guay-Woodford LM, Muecher G, Hopkins SD, Avner ED, Germino GG, Guillot AP, Herrin J, Holleman R, Irons DA, Primack W, Thompson PD, Waldo FB, Lunt PW, Zerres K. The severe perinatal form of autosomal recessive polycystic kidney disease maps to chromosome 6p21.1-p12: implications for genetic counseling. Am J Hum Genet 1995;56:1101–1107.
6. Roy S, Dillon MJ, Trompeter RS, Barratt TM. Autosomal recessive polycystic kidney disease: long-term outcome of neonatal survivors. Pediatr Nephrol 1997;11:302–306.
7. Hartung EA, Guay-Woodford LM. Autosomal recessive polycystic kidney disease: a hepatorenal fibrocystic disorder with pleiotropic effects. Pediatrics 2014;134:e833–e845.
8. Onuchic LF, Furu L, Nagasawa Y, Hou X, Eggermann T, Ren Z, Bergmann C, Senderek J, Esquivel E, Zeltner R, Rudnik-Schoneborn S, Mrug M, Sweeney W, Avner ED, Zerres K, Guay-Woodford LM, Somlo S, Germino GG. PKHD1, the polycystic kidney and hepatic disease 1 gene, encodes a novel large protein containing multiple immunoglobulin-like plexin-transcription-factor domains and parallel beta-helix 1 repeats. Am J Hum Genet 2002;70:1305–1317.
9. Harris PC, Rossetti S. Molecular genetics of autosomal recessive polycystic kidney disease. Mol Genet Metab 2004;81:75–85.
10. Menezes LF, Cai Y, Nagasawa Y, Silva AM, Watkins ML, Da Silva AM, Somlo S, Guay-Woodford LM, Germino GG, Onuchic LF. Polyductin, the PKHD1 gene product, comprises isoforms expressed in plasma membrane, primary cilium, and cytoplasm. Kidney Int 2004;66:1345–1355.
11. Ziegler WH, Soetje B, Marten LP, Wiese J, Burute M, Haffner D. Fibrocystin Is Essential to Cellular Control of Adhesion and Epithelial Morphogenesis. Int J Mol Sci 2020;21:5140.
12. O'Sullivan DA, Torres VE, Gabow PA, Thibodeau SN, King BF, Bergstralh EJ. Cystic fibrosis and the phenotypic expression of autosomal dominant polycystic kidney disease. Am J Kidney Dis 1998;32:976–983.
13. Persu A, Devuyst O, Lannoy N, Materne R, Brosnahan G, Gabow PA, Pirson Y, Verellen-Dumoulin C. CF gene and cystic fibrosis transmembrane conductance regulator expression in autosomal dominant polycystic kidney disease. J Am Soc Nephrol 2000;11:2285–2296.
14. Nakanishi K, Sweeney WE Jr, Macrae Dell K, Cotton CU, Avner ED. Role of CFTR in autosomal recessive polycystic kidney disease. J Am Soc Nephrol 2001;12:719–725.
15. Nauta J, Ozawa Y, Sweeney WE Jr, Rutledge JC, Avner ED. Renal and biliary abnormalities in a new murine model of autosomal recessive polycystic kidney disease. Pediatr Nephrol 1993;7:163–172.
16. Colombo C, Battezzati PM, Strazzabosco M, Podda M. Liver and biliary problems in cystic fibrosis. Semin Liver Dis 1998;18:227–235.
17. Tabibian JH, Masyuk AI, Masyuk TV, O'Hara SP, LaRusso NF. Physiology of cholangiocytes. Compr Physiol 2013;3:541–565.

18. Colombo C, Russo MC, Zazzeron L, Romano G. Liver disease in cystic fibrosis. J Pediatr Gastroenterol Nutr 2006;43(Suppl 1):S49–S55.

19. Lindblad A, Hultcrantz R, Strandvik B. Bile-duct destruction and collagen deposition: a prominent ultra-structural feature of the liver in cystic fibrosis. Hepatology 1992;16:372–381.

20. Balch WE, Roth DM, Hutt DM. Emergent properties of proteostasis in managing cystic fibrosis. Cold Spring Harb Perspect Biol 2011;3:a004499.

21. Skach WR. CFTR: new members join the fold. Cell 2006; 127:673–675.

22. Roth DM, Balch WE. Modeling general proteostasis: proteome balance in health and disease. Curr Opin Cell Biol 2011;23:126–134.

23. Borkan SC, Gullans SR. Molecular chaperones in the kidney. Annu Rev Physiol 2002;64:503–527.

24. Seit-Nebi AS, Gusev NB. Versatility of the small heat shock protein HSPB6 (Hsp20). Cell Stress Chaperones 2010;15:233–236.

25. Taipale M, Jarosz DF, Lindquist S. HSP90 at the hub of protein homeostasis: emerging mechanistic insights. Nat Rev Mol Cell Biol 2010;11:515–528.

26. Stiegler SC, Rubbelke M, Korotkov VS, Weiwad M, John C, Fischer G, Sieber SA, Sattler M, Buchner J. A chemical compound inhibiting the Aha1-Hsp90 chaperone complex. J Biol Chem 2017;292:17073–17083.

27. Murphy ME. The HSP70 family and cancer. Carcinogenesis 2013;34:1181–1188.

28. Gyrd-Hansen M, Nylandsted J, Jaattela M. Heat shock protein 70 promotes cancer cell viability by safeguarding lysosomal integrity. Cell Cycle 2004;3:1484–1485.

29. Kim YE, Hipp MS, Bracher A, Hayer-Hartl M, Hartl FU. Molecular chaperone functions in protein folding and proteostasis. Annu Rev Biochem 2013;82:323–355.

30. Van Goor F, Hadida S, Grootenhuis PD, Burton B, Stack JH, Straley KS, Decker CJ, Miller M, McCartney J, Olson ER, Wine JJ, Frizzell RA, Ashlock M, Negulescu PA. Correction of the F508del-CFTR protein processing defect in vitro by the investigational drug VX-809. Proc Natl Acad Sci U S A 2011;108:18843–18848.

31. Hanaoka K, Devuyst O, Schwiebert EM, Wilson PD, Guggino WB. A role for CFTR in human autosomal dominant polycystic kidney disease. Am J Physiol 1996; 270:C389–C399.

32. Hanaoka K, Guggino WB. cAMP regulates cell proliferation and cyst formation in autosomal polycystic kidney disease cells. J Am Soc Nephrol 2000;11:1179–1187.

33. Tradtrantip L, Sonawane ND, Namkung W, Verkman AS. Nanomolar potency pyrimido-pyrrolo-quinoxalinedione CFTR inhibitor reduces cyst size in a polycystic kidney disease model. J Med Chem 2009;52:6447–6455.

34. Verkman AS, Lukacs GL, Galietta LJ. CFTR chloride channel drug discovery–inhibitors as antidiarrheals and activators for therapy of cystic fibrosis. Curr Pharm Des 2006;12:2235–2247.

35. Yang B, Sonawane ND, Zhao D, Somlo S, Verkman AS. Small-molecule CFTR inhibitors slow cyst growth in polycystic kidney disease. J Am Soc Nephrol 2008; 19:1300–1310.

36. Li H, Sheppard DN. Therapeutic potential of cystic fibrosis transmembrane conductance regulator (CFTR) inhibitors in polycystic kidney disease. Biodrugs 2009; 23:203–216.

37. Yanda MK, Cha B, Cebotaru CV, Cebotaru L. Pharmacological reversal of renal cysts from secretion to absorption suggests a potential therapeutic strategy for managing autosomal dominant polycystic kidney disease. J Biol Chem 2019;294:17090–17104.

38. Gallagher AR, Esquivel EL, Briere TS, Tian X, Mitobe M, Menezes LF, Markowitz GS, Jain D, Onuchic LF, Somlo S. Biliary and pancreatic dysgenesis in mice harboring a mutation in Pkhd1. Am J Pathol 2008; 172:417–429.

39. Cheng SH, Gregory RJ, Marshall J, Paul S, Souza DW, White GA, O'Riordan CR, Smith AE. Defective intracellular transport and processing of CFTR is the molecular basis of most cystic fibrosis. Cell 1990;63:827–834.

40. Kumar A, Jagannathan N. Cytokeratin: A review on current concepts. Int J Orofac Biol 2018;2:6–11.

41. Grantham JJ. Mechanisms of progression in autosomal dominant polycystic kidney disease. Kidney Int Suppl 1997;63:S93–S97.

42. Seamon KB, Daly JW. Forskolin: a unique diterpene activator of cyclic AMP-generating systems. J Cyclic Nucleotide Res 1981;7:201–224.

43. Ghelani DP, Schneider-Futschik EK. Emerging cystic fibrosis transmembrane conductance regulator modulators as new drugs for cystic fibrosis: a portrait of in vitro pharmacology and clinical translation. ACS Pharmacol Transl Sci 2019;3:4–10.

44. Uc A, Giriyappa R, Meyerholz DK, Griffin M, Ostedgaard LS, Tang XX, Abu-El-Haija M, Stoltz DA, Ludwig P, Pezzulo A, Abu-El-Haija M, Taft P, Welsh MJ. Pancreatic and biliary secretion are both altered in cystic fibrosis pigs. Am J Physiol Gastrointest Liver Physiol 2012;303:G961–G968.

45. Nakashima T, Ishii T, Tagaya H, Seike T, Nakagawa H, Kanda Y, Akinaga S, Soga S, Shiotsu Y. New molecular and biological mechanism of antitumor activities of KW–2478, a novel nonansamycin heat shock protein 90 inhibitor, in multiple myeloma cells. Clin Cancer Res 2010;16:2792–2802.

46. Wen W, Liu W, Shao Y, Chen L. VER–155008, a small molecule inhibitor of HSP70 with potent anti-cancer activity on lung cancer cell lines. Exp Biol Med (Maywood) 2014;239:638–645.

47. Ostedgaard LS, Meyerholz DK, Chen JH, Pezzulo AA, Karp PH, Rokhlina T, Ernst SE, Hanfland RA, Reznikov LR, Ludwig PS, Rogan MP, Davis GJ, Dohrn CL, Wohlford-Lenane C, Taft PJ, Rector MV, Hornick E, Nassar BS, Samuel M, Zhang Y, Richter SS, Uc A, Shilyansky J, Prather RS, McCray PB Jr, Zabner J, Welsh MJ, Stoltz DA. The DeltaF508 mutation causes CFTR misprocessing and cystic fibrosis-like disease in pigs. Sci Transl Med 2011;3:74ra24.

48. Brodsky JL. The protective and destructive roles played by molecular chaperones during ERAD (endoplasmic-reticulum-associated degradation). Biochem J 2007; 404:353–363.

49. Yanda MK, Liu Q, Cebotaru L. A potential strategy for reducing cysts in autosomal dominant polycystic kidney disease with a CFTR corrector. J Biol Chem 2018; 293:11513–11526.

50. Mymrikov EV, Seit-Nebi AS, Gusev NB. Large potentials of small heat shock proteins. Physiol Rev 2011; 91:1123–1159.

51. Kamada M, So A, Muramaki M, Rocchi P, Beraldi E, Gleave M. Hsp27 knockdown using nucleotide-based therapies inhibit tumor growth and enhance chemotherapy in human bladder cancer cells. Mol Cancer Ther 2007;6:299–308.

52. Nahomi RB, Palmer A, Green KM, Fort PE, Nagaraj RH. Pro-inflammatory cytokines downregulate Hsp27 and cause apoptosis of human retinal capillary endothelial cells. Biochim Biophys Acta 2014;1842:164–174.

53. Lopes-Pacheco M, Boinot C, Sabirzhanova I, Morales MM, Guggino WB, Cebotaru L. Combination of Correctors Rescue DeltaF508-CFTR by Reducing Its Association with Hsp40 and Hsp27. J Biol Chem 2015; 290:25636–25645.

54. Sabirzhanova I, Lopes Pacheco M, Rapino D, Grover R, Handa JT, Guggino WB, Cebotaru L. Rescuing Trafficking Mutants of the ATP-binding Cassette Protein, ABCA4, with Small Molecule Correctors as a Treatment for Stargardt Eye Disease. J Biol Chem 2015;290:19743–19755.

55. Yanda MK, Guggino WB, Cebotaru L. A new role for heat shock factor 27 in the pathophysiology of Clostridium difficile toxin B. Am J Physiol Gastrointest Liver Physiol 2020;318:G120–G129.

56. Doshi BM, Hightower LE, Lee J. HSPB1, actin filament dynamics, and aging cells. Ann N Y Acad Sci 2010; 1197:76–84.

57. Mai W, Chen D, Ding T, Kim I, Park S, Cho SY, Chu JS, Liang D, Wang N, Wu D, Li S, Zhao P, Zent R, Wu G. Inhibition of Pkhd1 impairs tubulomorphogenesis of cultured IMCD cells. Mol Biol Cell 2005;16:4398–4409.

58. Proia D, Golemis E, Seeger-Nukpezah T. Treating polycystic kidney disease with hsp90 inhibitory compounds. , Available at: https://patentscope.wipo.int/search/en/detail.jsf?docId=WO2014063080 Accessed October 8, 2015.

59. Seeger-Nukpezah T, Proia DA, Egleston BL, Nikonova AS, Kent T, Cai KQ, Hensley HH, Ying W, Chimmanamada D, Serebriiskii IG, Golemis EA. Inhibiting the HSP90 chaperone slows cyst growth in a mouse model of autosomal dominant polycystic kidney disease. Proc Natl Acad Sci U S A 2013;110:12786–12791.

60. Bertolini A, Bodewes FAJA, Slae M, Wilschanski M. Hepatobiliary Involvement in Cystic Fibrosis. In: Davis SD, Rosenfeld M, Chmiel J, eds. Cystic Fibrosis. Cham, Switzerland: Springer International, 2020; 2020:299–320, Accessed October 8, 2015.

61. Bidaud-Meynard A, Bossard F, Schnur A, Fukuda R, Veit G, Xu H, Lukacs GL. Transcytosis maintains CFTR apical polarity in the face of constitutive and mutation-induced basolateral missorting. J Cell Sci 2019;132:jcs226886.

62. Buchholz B, Faria D, Schley G, Schreiber R, Eckardt K-U, Kunzelmann K. Anoctamin 1 induces calcium-activated chloride secretion and proliferation of renal cyst–forming epithelial cells. Kidney Int 2014;85:1058–1067.

63. Fuller CM, Benos DJ. CFTR! Am J Physiol 1992; 263:C267–C286.

64. Skach WR. Defects in processing and trafficking of the cystic fibrosis transmembrane conductance regulator. Kidney Int 2000;57:825–831.

65. Elborn JS, Ramsey BW, Boyle MP, Konstan MW, Huang X, Marigowda G, Waltz D, Wainwright CE. Efficacy and safety of lumacaftor/ivacaftor combination therapy in patients with cystic fibrosis homozygous for Phe508del CFTR by pulmonary function subgroup: a pooled analysis. Lancet Respir Med 2016;4:617–626.

66. Garcia-Gonzalez MA, Menezes LF, Piontek KB, Kaimori J, Huso DL, Watnick T, Onuchic LF, Guay-Woodford LM, Germino GG. Genetic interaction studies link autosomal dominant and recessive polycystic kidney disease in a common pathway. Hum Mol Genet 2007; 16:1940–1950.

67. Yanda MK, Liu Q, Cebotaru V, Guggino WB, Cebotaru L. Histone deacetylase 6 inhibition reduces cysts by decreasing cAMP and Ca(2+) in knock-out mouse models of polycystic kidney disease. J Biol Chem 2017; 292:17897–17908.